The Plant Cell, Vol. 29: 2570–2580, October 2017, www.plantcell.org © 2017 ASPB.

Fusicoccin Activates KAT1 Channels by Stabilizing Their Interaction with 14-3-3 Proteins[OPEN]

Andrea Saponaro,[a] Alessandro Porro,[a] Antonio Chaves-Sanjuan,[a] Marco Nardini,[a] Oliver Rauh,[b] Gerhard Thiel,[b] and Anna Moroni[a,c,1]

[a] Department of Biosciences, University of Milan, 20133 Milan, Italy
[b] Plant Membrane Biophysics, Technical University Darmstadt, 64287 Darmstadt, Germany
[c] Institute for Biophysics-Milan, Consiglio Nazionale delle Ricerche, 20133 Milan, Italy

ORCID IDs: 0000-0001-5035-5174 (A.S.); 0000-0003-3287-9024 (A.C.-S.); 0000-0002-3718-2165 (M.N.); 0000-0002-2335-1351 (G.T.); 0000-0002-1860-460X (A.M.)

Plants acquire potassium (K^+) ions for cell growth and movement via regulated diffusion through K^+ channels. Here, we present crystallographic and functional data showing that the K^+ inward rectifier KAT1 (K^+ *Arabidopsis thaliana* 1) channel is regulated by 14-3-3 proteins and further modulated by the phytotoxin fusicoccin, in analogy to the H^+-ATPase. We identified a 14-3-3 mode III binding site at the very C terminus of KAT1 and cocrystallized it with tobacco (*Nicotiana tabacum*) 14-3-3 proteins to describe the protein complex at atomic detail. Validation of this interaction by electrophysiology shows that 14-3-3 binding augments KAT1 conductance by increasing the maximal current and by positively shifting the voltage dependency of gating. Fusicoccin potentiates the 14-3-3 effect on KAT1 activity by stabilizing their interaction. Crystal structure of the ternary complex reveals a noncanonical binding site for the toxin that adopts a novel conformation. The structural insights underscore the adaptability of fusicoccin, predicting more potential targets than so far anticipated. The data further advocate a common mechanism of regulation of the proton pump and a potassium channel, two essential elements in K^+ uptake in plant cells.

INTRODUCTION

The activity and number of ion channels in the plasma membrane is tightly controlled by second messengers and regulatory proteins (Blatt, 2000). In the case of KAT1, the prototype inward rectifying potassium (K^+) channel of plant cells, it is well established that 14-3-3 proteins modulate aspects of its life cycle related to membrane trafficking as well as to its activity at the plasma membrane (Duby and Boutry, 2009; Sottocornola et al., 2008). The 14-3-3 proteins are a well-known class of auxiliary proteins that regulate trafficking and activity of many membrane proteins by means of protein-protein interaction (Smith et al., 2011). In the case of the plant H^+-ATPase, the interaction of 14-3-3 with the cytosolic C terminus of the H^+ pump is known in atomic detail (Ottmann et al., 2007), as is the molecular mechanism mediating upregulation of the H^+-ATPase by the fungal toxin fusicoccin (FC), the best known activator of the H^+ pump and a potent enhancer of stomata opening (Aducci et al., 1995). FC is a small amphipatic molecule that binds to the protein complex formed by the H^+ pump C terminus and 14-3-3 proteins and strongly stabilizes the interaction of the two partners (Würtele et al., 2003; Paiardini et al., 2014). Currently it is not known how the activity of the KAT1 channel is integrated in this scenario. Some indirect evidence for a regulatory modulation of KAT1 by the 14-3-3 proteins can be anticipated from data, which show that activity and trafficking of the channel are promoted by an overexpression of 14-3-3 proteins (Sottocornola et al., 2006, 2008). So far, direct binding of 14-3-3 proteins to the KAT1 channel has not been demonstrated.

In this work, we examine the molecular details of the interaction between 14-3-3 proteins and KAT1. After the identification of a 14-3-3 binding sequence at the C terminus of KAT1, we cocrystallized the corresponding KAT1 peptide with 14-3-3 to identify the atomic determinants of their interaction. Further structural and functional data show that this interaction is also stabilized by FC, as is the interaction between 14-3-3 and the H^+ pump. The surprise of this discovery is 2-fold: (1) Despite the wealth of functional information on the FC toxin (Marrè, 1979), KAT1 was never suspected to be a direct target of FC; and (2) even more surprising, FC was so far reported to stabilize 14-3-3 complexes only in the presence of a C-terminal small hydrophobic residue in the 14-3-3 partner protein. Our structural data now show that FC is able to stabilize the KAT1:14-3-3 complex even though the C-terminal residue of KAT1 is the polar amino acid asparagine. Altogether, our results constitute the first functional and atomic description of the regulation of KAT1 by 14-3-3 proteins and FC.

RESULTS

14-3-3 Binding to KAT1 Is Regulated by S676 Phosphorylation

14-3-3 proteins engage a direct interaction with their partners by binding to specific phosphoserine/threonine motifs. In membrane proteins, 14-3-3 binding motifs can be found anywhere in cytosolic

[1] Address correspondence to anna.moroni@unimi.it.
The author responsible for distribution of materials integral to the findings presented in this article in accordance with the policy described in the Instructions for Authors (www.plantcell.org) is: Anna Moroni (anna.moroni@unimi.it).
[OPEN]Articles can be viewed without a subscription.
www.plantcell.org/cgi/doi/10.1105/tpc.17.00375

domains (MODE I and II) or at the very end of the C terminus (MODE III). In the last case the phosphorylated residue is generally at the penultimate position of the protein sequence (Johnson et al., 2010). The KAT1 sequence reveals three potential phosphorylation-dependent 14-3-3 binding motifs in the C terminus: RSS**S**E579 belongs to MODE I, RDFK**S**M521 to MODE II, and **S**N677 to MODE III (the phosphorylated residue is in bold). KAT1 has the typical architecture of tetrameric Kv channels. Each subunit comprises six transmembrane domains and cytosolic N and C termini (Whicher and MacKinnon, 2016). The latter hosts a cyclic nucleotide binding homology domain (CNBHD) and a downstream so-called KHA domain (Marten and Hoshi, 1997; Ehrhardt et al., 1997). The potential MODE I and MODE II phosphorylation sites are located between the CNBHD and KHA domains, while the MODE III site is at the C-terminal end of the protein (Figure 1A).

We tested the relevance of the three motifs for 14-3-3 binding by mutating their serine into an alanine (S520A, S578A, and S676A) to prevent phosphorylation and, therefore, the interaction with 14-3-3 proteins. As a readout, we analyzed the effect of 14-3-3 proteins on KAT1 current by transiently expressing the channel in

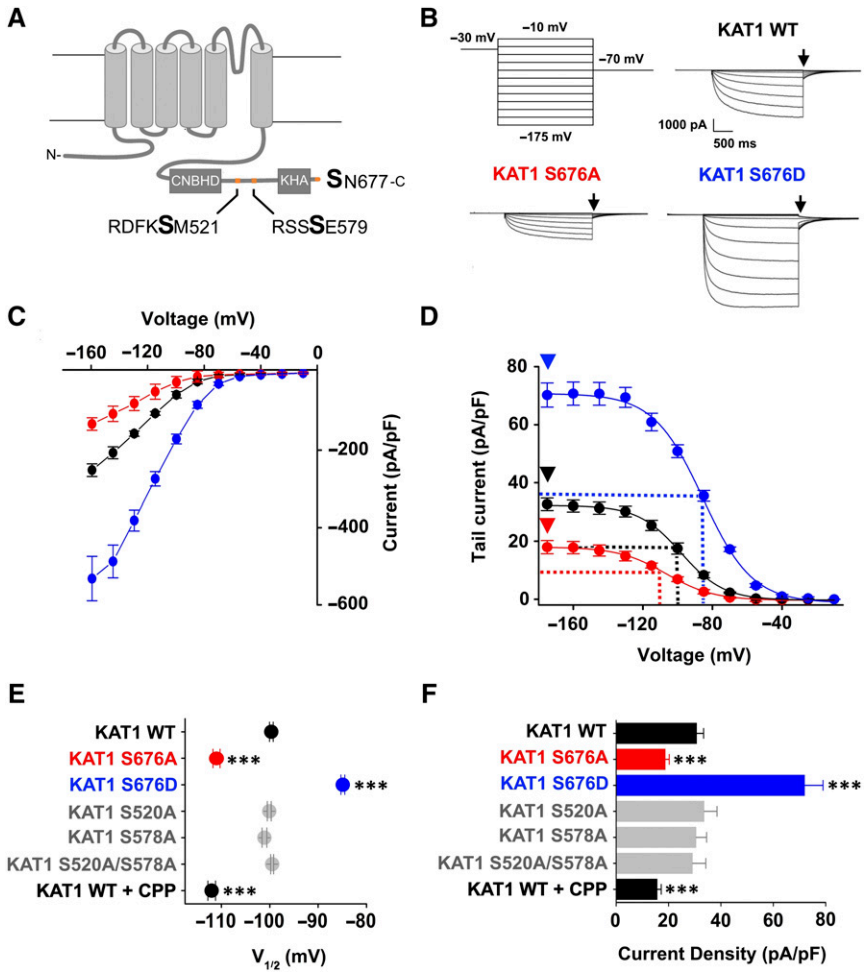

Figure 1. Identification of the 14-3-3 Binding Motif in the KAT1 Channel.

(A) Cartoon representation of one of the four subunits forming the KAT1 channel. The principal cytosolic domains are labeled: cyclic nucleotide binding homology domain (CNBHD) and oligomerization domain (KHA). The position of two 14-3-3 binding motifs (RDFK**S**M521 and RSS**S**E579) is indicated by an arrow, while the third one (**S**N677) is at the C terminus. The presumably phosphorylated serine is in bold.

(B) Representative current traces of KAT1 wild-type and S676A and S676D mutant channels recoded in HEK 293T cells using the indicated voltage protocol. Black arrows indicate the current selected for analysis in **(D)**.

(C) Mean steady state current/voltage relations of KAT1 wild type (black), S676A (red), and S676D (blue).

(D) Activation curves of KAT1 wild type (black), S676A (red), and S676D (blue) channels obtained from tail currents collected at −70 mV (see arrow **[B]**). The currents were normalized for the cell capacitance and plotted (changed in sign) as a function of test voltages. Dashed lines indicate the half activation potential ($V_{1/2}$) value, while arrowheads indicate the current density value at saturation, plotted in **(E)** and **(F)**, respectively.

(E) and **(F)** Half activation potential ($V_{1/2}$) **(E)** and current density (pA/pF) **(F)** of KAT1 wild type and mutants. Data are presented as means ± SE. Number of cells (*n*) was ≥ 10. Statistical analysis performed with *t* test (***P < 0.001 and *P < 0.05).

mammalian HEK 293T cells. It is well established that animal 14-3-3 proteins activate KAT1 conductance in two ways: by increasing the current density (i.e., the number of active channels in the plasma membrane) and by increasing the channel open probability at a given voltage. As a result of 14-3-3 binding, the channel maximal current increases and the half activation potential, the voltage value at which 50% of the channels are open ($V_{1/2}$), shifts positive of ~10 mV (Sottocornola et al., 2006, 2008). All mutants generated voltage-dependent, slowly activating, inward rectifying K^+ currents, typical of the wild-type KAT1 channel (Figure 1B). S520A and S578A, either alone or in combination, did not induce any apparent difference from the wild-type channel current (Table 1). S676A, on the contrary, displayed a strong reduction in current (Figure 1B), a typical sign of lack of 14-3-3 regulation. As shown by the mean I/V curve plotted in Figure 1C, the mutation caused a current reduction of ~50% compared with the wild-type channel. The activation curves, obtained from tail currents at –70 mV (arrow in Figure 1B) were normalized for the cell capacitance and plotted as a function of the preconditioning voltage (Figure 1D). Fitting the data to the Boltzmann equation (solid line; see Methods for equation) yielded $V_{1/2}$ values, plotted in Figure 1E for all mutants. Maximal current values were calculated at the saturating voltage of –175 mV (arrowhead in Figure 1D) and plotted in Figure 1F. Inverse slope coefficient (S), a Boltzmann parameter that expresses the steepness of the voltage dependency, did not change significantly among mutants and the wild type (Table 1). The reduction in current of the S676A mutant is due to a left shift of the $V_{1/2}$ value of ~10 mV (Figure 1E). Figure 1F also shows a reduction (of ~30%) in current density, which is significantly different from the wild type. These data suggest that phosphorylation of S676 is essential for 14-3-3 regulation of KAT1. To confirm this hypothesis, we introduced the phosphomimic mutation S676D. As expected, this mutation increased the current by potentiating both voltage-dependent channel opening (~15 mV right shift in $V_{1/2}$) and the number of channels in the plasma membrane (2.5-fold increase of current density) when compared with the wild type (Figures 1B to 1F, Table 1).

To prove that the effect of 14-3-3 proteins was due to the direct interaction of the proteins with the KAT1 C terminus, we set up a competition experiment in which we displaced the binding of 14-3-3 proteins from the channel by supplying the synthetic C terminus phosphorylated peptide (CPP) YFS**pS**N of KAT1. We dialyzed CPP in the cytosol of the cell during patch recordings by dissolving it (10 μM) in the intracellular solution of the pipette. The data show that perfusion of CPP into the cytoplasm of HEK 293T cells expressing wild-type KAT1 channels caused the same effects on $V_{1/2}$ and current density of the S676A mutation, thus confirming that CPP prevents 14-3-3 proteins binding to the channel (Figures 1E and 1F, Table 1).

In summary, our data show that 14-3-3 proteins directly interact with KAT1 at a newly discovered MODE III binding site requiring phosphorylation of S676 in the penultimate position at the channel C terminus.

14-3-3:KAT1 C Terminus Complex

To explain the interaction of KAT1 and 14-3-3 proteins in atomic detail, we cocrystallized tobacco (*Nicotiana tabacum*) 14-3-3 proteins isoform c (14-3-3c) with CPP. Crystals diffracted to a maximum resolution of 2.35 Å (Table 2). A longer version of the synthetic peptide, extended by two amino acids at the N terminus (CPP7: HLYFS**pS**N), was also tested, and since the overall structure of the two complexes is nearly identical (Supplemental Figures 1 and 2), we focused only on the structure of 14-3-3c in complex with CPP for simplicity (Figure 2). 14-3-3c proteins form a cup-like dimer (Figure 2A) with a symmetry-related mate, as

Table 1. Analysis of Currents Recorded in Whole-Cell Configuration from Wild-Type and Mutant KAT1 Channels

	$V_{1/2}$	S	Current Density	*n*
KAT1 WT	−99.5 ± 0.5 mV	13.5 ± 0.5	32.1 ± 4.2 pA/pF	65
KAT1 WT + FC	−82.8 ± 0.5 mV	13.9 ± 0.6	60 ± 1.9 pA/pF	31
KAT1 S676A	−110 ± 0.7 mV	13.1 ± 0.5	18.2 ± 2.3 pA/pF	25
KAT1 S676A + FC	−112.4 ± 0.9 mV	12.8 ± 0.4	18.9 ± 2.5 pA/pF	8
KAT1 S676D	−84.9 ± 0.4 mV	12.3 ± 0.4	72 ± 7 pA/pF	13
KAT1 S520A	−100.1 ± 0.4 mV	12.2 ± 0.3	33.6 ± 4.9 pA/pF	11
KAT1 S578A	−101.1 ± 0.5 mV	13.3 ± 0.5	30.5 ± 4 pA/pF	10
KAT1 S520A/S578A	−99.5 ± 0.3 mV	14.4 ± 0.3	29.1 ± 5.1 pA/pF	10
KAT1 F674A	−99.1 ± 0.4 mV	13.6 ± 0.4	33 ± 5 pA/pF	10
KAT1 WT + CPP	−112 ± 0.8 mV	13.5 ± 0.6	16 ± 1.5 pA/pF	10
KAT1 P678	−100 ± 0.9 mV	14.6 ± 0.8	31.6 ± 1.4 pA/pF	8
KAT1 P678 + FC	−84.6 ± 0.8 mV	15 ± 0.8	67 ± 1.8 pA/pF	9
KAT1 ENS680	−100.5 ± 0.5 mV	14.4 ± 0.5	36.5 ± 0.5 pA/pF	8
KAT1 ENS680 + FC	−86.7 ± 0.4 mV	13.4 ± 0.4	66 ± 2 pA/pF	8
KAT1 N677V	−102.6 ± 0.4 mV	13.7 ± 0.3	30.9 ± 3.9 pA/pF	8
KAT1 N677V + FC	−83.1 ± 0.6 mV	14 ± 0.5	60.9 ± 2.3 pA/pF	8
KAT1 N677V/P680	−100.4 ± 0.9 mV	14.9 ± 0.8	32.6 ± 4.2 pA/pF	8
KAT1 N677V/P680+ FC	−100.9 ± 0.7 mV	15.3 ± 0.7	28.8 ± 2.3 pA/pF	8

$V_{1/2}$ and S are the parameters obtained by the Boltzmann fit of the activation curve and correspond to the half activation voltage and the inverse slope factor, respectively. Current density was calculated by dividing the current value recorded at –135 mV for the cell capacitance. *n* is the number of cells. WT, wild type.

Table 2. Diffraction Data Collection and Refinement Statistics

Data Set	14-3-3c:CPP	14-3-3c:CPP7	14-3-3c:CPP:FC
Data collection			
Space group	$P6_522$	$P6_522$	$P2_12_12_1$
Cell dimensions			
a, b, c (Å)	110.18, 110.18, 136.69	109.03, 109.03, 136.71	99.81, 165.66, 170.55
α, β, γ (°)	90.0, 90.0, 120.0	90.0, 90.0, 120.0	90.0, 90.0, 90.0
Wavelength (Å)	0.96770	0.96770	0.97625
Resolution (Å)	47.71–2.35 (2.43–2.35)	47.21–2.07 (2.13–2.07)	48.32–3.30 (3.42–3.30)
$^{\#}R_{pim}$	0.045 (0.365)	0.037 (0.356)	0.132 (0.304)
$^{+}CC_{1/2}$	0.971 (0.706)	0.999 (0.523)	0.978 (0.407)
$<I/\sigma(I)>$	15.2 (5.1)	18.3 (5.1)	5.6 (2.7)
Completeness (%)	100 (100)	99.8 (99.8)	100 (100)
Wilson B-factor	32.28	29.44	45.76
Redundancy	39.0 (27.7)	40.9 (39.8)	7.5 (7.6)
Refinement			
Resolution (Å)	42.89–2.35 (2.43–2.35)	44.63–2.07 (2.14–2.07)	47.89-3.30 (3.41–3.30)
Number of reflections	21,014 (2,044)	29,779 (2,904)	43,249 (4,259)
R_{work}/R_{free}	0.195/0.245 (0.340/0.338)	0.200/0.247 (0.327-0.357)	0.241/0.306 (0.291/0.381)
Number of molecules			
Copies in the AU	1	1	8
Protein residues	245	247	1898
FSC molecules	–	–	7
PEG molecules	–	3	–
GOL molecules	–	1	–
ACT molecules	1	1	–
Water molecules	148	185	101
Average B factors (Å^2)	51.5	46.3	63.4
Average B factors (FSC) (Å^2)	–	–	49.9
RMSD			
Bond lengths (Å)	0.013	0.015	0.002
Bond angles (°)	1.15	1.22	0.51
Ramachandran plot statistics	99% in favored	98% in favored	98% in favored
	0.0% outliers	0.0% outliers	0.0% outliers

Highest-resolution shell is shown in parentheses. $^{+}CC_{1/2}$ is the correlation coefficient of the mean intensities between two random half-sets of data. RMSD, root mean square deviation. $^{\#}R_{p.i.m.} = \sum_{hkl}\sqrt{1/n-1}\sum_{j=1}^{n}|I_{hkl} - \langle I_{hkl}\rangle|/\sum_{hkl}\sum_{j}I_{hkl,j}$.

previously described for other 14-3-3 structures (Ottmann et al., 2007). CPP binds in an extended conformation in the canonical 14-3-3 binding groove (Figure 2A). The phosphoserine of CPP establishes two electrostatic interactions with R63 and R136 as well as a hydrogen bond with Y137 of 14-3-3c (Figure 2B). These residues are highly conserved in 14-3-3 proteins as they bind to the phosphate moiety of the target peptides (Paiardini et al., 2014). Additionally, CPP interacts with several polar and hydrophobic residues of the 14-3-3c binding groove (Figure 2B).

Fusicoccin Potentiates 14-3-3:KAT1 Interaction

The phytotoxin FC is a diterpenoid glycoside that binds to the complex formed by 14-3-3 proteins with their phosphorylated targets. Binding of FC stabilizes the protein-protein complex leading to an apparent irreversibility of 14-3-3 binding. So far, the best characterized targets of FC are the plant H^+-ATPase and the animal TASK1 channel. In both cases, the MODE III phosphopeptide of the 14-3-3 target protein ends with the small hydrophobic amino acid valine that establishes crucial interactions with the hydrophobic rings of FC (Würtele et al., 2003; Anders et al., 2013). The presence of a C-terminal small hydrophobic residue is considered necessary for FC binding (Paiardini et al., 2014). Important to note in this context is that the MODE III binding motif of KAT1 does not end with such a canonical hydrophobic residue, but with the hydrophilic asparagine. For this reason, KAT1 was not considered a potential FC target.

Much to our surprise, we found that pretreating (30 min) HEK 293T cells expressing KAT1 with FC (10 μM) caused a positive shift in the voltage dependency of the channel (~13 mV right shift in $V_{1/2}$) and increased the current density (~2-fold) to the same extent as did the phosphomimic mutation S676D (compare Figures 3A and 3B with Figures 1E and 1F; see Table 1 for details). The dual effect of FC indicates that FC, in combination with 14-3-3 proteins, alters two functional properties of the channel: its voltage dependency and the maximal current. While the former can be explained by an effect of FC on channel gating, the latter can in principle originate from an increase of the unitary conductance of the channel or from an increase in the number of channels in the membrane. To discriminate between the two possibilities, we performed a nonstationary noise analysis (Liu et al., 2016). HEK 293T cells expressing KAT1 were stepped in the absence or

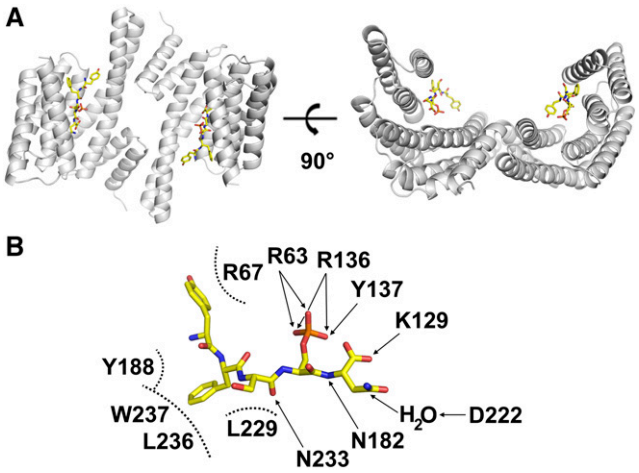

Figure 2. Crystallographic Structure of 14-3-3 in Complex with the Phosphorylated CPP of KAT1.

(A) Ribbon representation, in two different orientations, of the dimeric 14-3-3c protein from tobacco (gray ribbon) bound to KAT1 C terminus phosphorylated peptide CPP (yellow sticks).

(B) Schematic representation of the interactions between 14-3-3c residues (labeled in black) and CPP residues YFSpSN. Arrows indicate polar interactions, while dashed half circles indicate hydrophobic interactions.

presence of 10 μM FC 100 times from –40 mV to –160 mV. Figure 3C shows the resulting variance between successive pulses as a function of the mean current. A fit of the bell-shaped data with a parabolic function yields a mean value of 0.29 pA ± 0.1 pA ($n = 5$) for the single-channel current in the absence of FC and 0.33 pA ± 0.15 pA ($n = 4$) in its presence. The small difference between the two values is statistically not significant (P = 0.6 in a Student's *t* test). The results of this analysis show that the FC-generated increase in the maximal current does not result from a change in the unitary conductance, but from the number of channels in the membrane.

This suggests that FC has a stabilizing effect on the complex formed between 14-3-3 proteins and the MODE III motif of KAT1, even in the absence of a C-terminal hydrophobic residue. Thus, the phospho-null mutant S676A should result, in this case too, in FC-insensitive channels. Expression of the mutant channel in HEK 293T cells showed that this is indeed the case: The addition of FC had no effect on the current and was unable to revert the left shift in $V_{1/2}$ (Figure 3A) and the decrease in maximal current introduced by the mutation (Figure 3B, Table 1).

The stabilizing effect of FC on the complex formed by 14-3-3c and CPP was further quantified by isothermal titration calorimetry (ITC) (Wiseman et al., 1989). Figure 3E reports a control experiment in which CnPP, the nonphosphorylated peptide, was injected into a sample cell containing 14-3-3c, resulting in no heat changes. This confirms that the peptide, when not phosphorylated, does not bind to the proteins, as predicted by the previous experiment with the KAT1 mutant S676A (see Figure 1). Figures 3F and 3G show results obtained when the experiment was repeated with the phosphorylated peptide, CPP, in the absence (Figure 3F) and presence (Figure 3G) of FC. Analysis of the data using a single binding site model (solid line in Figures 3F and 3G; see Methods for equation), yielded mean K_d values of 0.69 ± 0.05 μM and of 0.27 ± 0.02 μM in the absence and presence of FC, respectively.

Notably, the stabilizing effect of FC on CCP binding to 14-3-3c (2.5-fold) is lower than that reported for the H^+ pump phosphopeptide binding (>10-fold) (Würtele et al., 2003; Paiardini et al., 2014), suggesting that FC may bind the CPP of KAT1 in an alternative manner, likely due to the presence of the polar asparagine in the last position that replaces the more commonly found valine.

Structural Basis of the Fusicoccin Effect on the 14-3-3: KAT1 Complex

To understand the interaction between 14-3-3c, CPP, and FC in atomic detail, we solved the crystallographic structure of the ternary complex at 3.3-Å resolution (Supplemental Figures 3 and 4; Table 2). FC is accommodated in the binding groove next to the C terminus of the CPP peptide and makes extensive contact with 14-3-3c (Figure 4). The hydrophobic diterpene moiety of FC is buried inside the 14-3-3 groove where it performs mainly hydrophobic interactions with V53, F126, P174, I175, L225, and I226 (Figure 4A) and two hydrogen bonds with D222 and S52 (Figure 4B). The glycosidic moiety of FC, which is more exposed to the solvent than the rest of the molecule, is also anchored to D222 of 14-3-3c via hydrogen bonds (Figure 4B).

In stark contrast to all known complexes, FC acquires in our structure an orientation within the 14-3-3 groove that has not been seen before, in either the ternary complexes with other phosphopeptides or in the binary FC:14-3-3 complex (Würtele et al., 2003; Anders et al., 2013) (Figures 4C and 4D). This unusual conformation of FC is imposed by the presence of the terminal asparagine in CPP that establishes a hydrogen bond with the hydroxyl group of FC at position C12 of the diterpene moiety (red arrow in Figure 4B).

Notably, the stabilizing effect of FC in our complex is due to the direct polar contact that FC provides to CPP and no crystal contacts constrain this FC conformation (for more details, see Supplemental Figure 4). This is unique to our structure because in other ternary complexes, for example, that with the C terminus peptide of the H^+ pump (Figure 4C; Würtele et al., 2003), FC confers stabilization by providing an extra hydrophobic pocket for the side chain of the C-terminal valine.

Our structural data confirm that FC is a rather versatile molecule and can rearrange in order to face chemically different surrounding protein residues. Notably, the KAT1-induced rearrangement of the FC moiety is further reflected in the thermodynamic parameters measured in ITC. The increase in the entropy of the binding reaction observed when CPP binds to 14-3-3c preincubated with FC (Supplemental Figure 5) likely indicates a solvent release entropy gain caused by the rearrangement of FC within the 14-3-3 cavity. Moreover, this FC rearrangement within the 14-3-3 groove can explain the weaker stabilizing effect of FC on KAT1 phosphopeptide compared with that on the H^+ pump, which, indeed, induces only minor rearrangements in FC (Würtele et al., 2003).

Functional Validation of FC Binding Modality

It is generally believed that FC stabilizes the complex between 14-3-3 proteins and MODE III motifs that are found at the end of

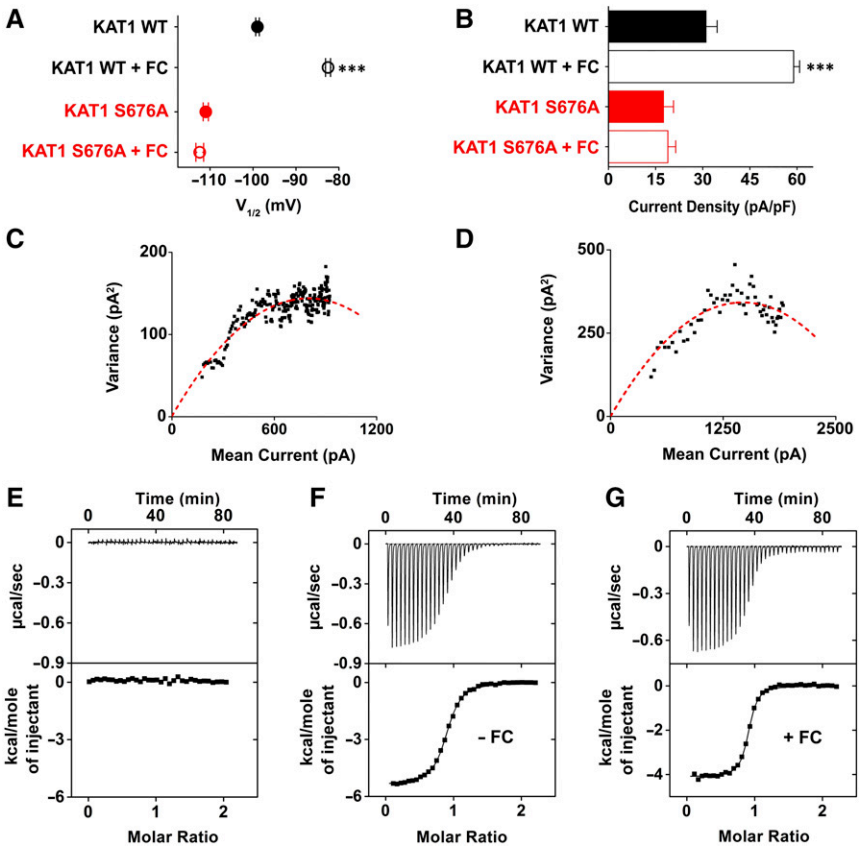

Figure 3. FC Activates KAT1 Channels by Stabilizing the Complex with 14-3-3 Proteins.

(A) and **(B)** Effect of 10 μM FC on KAT1 currents recorded in HEK 293T cells. Half activation potential ($V_{1/2}$) **(A)** and tail current density (pA/pF) **(B)** of KAT1 wild type and the KAT1 S676A mutant. Data are presented as mean ± SE. Number of cells (n) ≥ 8. Statistical analysis performed with t test (***$P < 0.001$).
(C) and **(D)** Noise analysis of KAT wild type channel ± FC in bath medium. Variance as a function of mean current from cells in the absence **(C)** and presence **(D)** of 10 μM FC. Dashed curves represent data fit to Equation 4 (see Methods), yielding, in the preset examples, a unitary current of 0.39 pA and 0.45 pA for **(C)** and **(D)**, respectively.
(E) to **(G)** CnPP and CPP binding to purified 14-3-3c proteins measured by ITC. Upper panel, heat changes (μcal/s) during successive injections of 10 μL of CnPP (500 μM) **(E)** and of CPP (500 μM) (**[F]** and **[G]**) into the chamber containing 14-3-3c (50 μM) in the absence (**[E]** and **[F]**) and presence **(G)** of 250 μM FC. Lower panel: binding curve obtained from data displayed in the upper panel. The peaks were integrated, normalized to CnPP or CPP concentration, and plotted against the molar ratio peptide:14-3-3c. Solid line represents a nonlinear least-squares fit to a single-site binding model (see Methods) yielding, in the preset examples, a K_d of 0.67 ± 0.03 μM and 0.28 ± 0.02 μM for **(F)** and **(G)**, respectively. Each experiment was repeated three times.

a protein sequence (Paiardini et al., 2014). In all crystal structures obtained so far, FC occupies the end of the 14-3-3 groove, suggesting that any downstream extension of the bound phospho-peptide would cause a steric clash with the toxin, specifically with the hydroxyl group on C12. For this reason, FC cannot stabilize the complex with MODE I and MODE II motifs because these 14-3-3 binding peptides are not found at the very end, but in the middle of proteins (Ottmann et al., 2009). In our crystal structure, though, the critical C12 hydroxyl group of FC is rearranged by the hydrogen bond that forms with the C-terminal asparagine residue (Figure 4C). Thus, we predict that, in this specific case in which an asparagine is in position +1 (one residue after the phosphorylated residue), FC binding is no longer restricted to the very C terminus of a protein and it should tolerate downstream extension of the amino acid sequence.

To test this hypothesis, we extended the full-length sequence of KAT1 by one residue at the C terminus and the mutant channel was then tested for the FC effect on the current. In the first case, we added a proline residue at the KAT1 C terminus (KAT1 P678 mutant) because proline is commonly found in position +2 (two residues after the phosphorylated amino acid) of MODE I and MODE II sites (Johnson et al., 2010). As predicted, the KAT1 P678 mutant was able to respond to FC that shifted the $V_{1/2}$ and increased the current density to the same extent as wild-type channels (Figures 5A and 5B, Table 1).

To test a nonconventional 14-3-3 binding motif (Johnson et al., 2010), we extended the sequence by adding three residues (ENS) at the C terminus. These are the last three residues of a similar channel, KAT2, that does not have a MODE III binding motif for 14-3-3 and does not respond to FC (Supplemental Figure 6). Functional testing of this mutant (KAT1 ENS680) showed that this

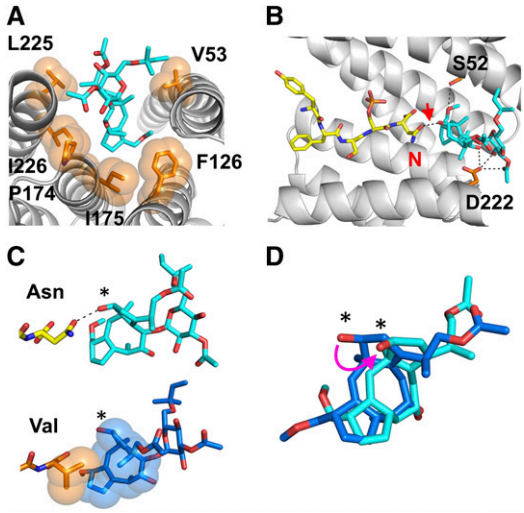

Figure 4. Crystal Structure of 14-3-3c:CPP:FC Ternary Complex.

(A) and **(B)** Detailed view on the interaction of FC (cyan sticks) with 14-3-3c (gray ribbon) and CPP (YFSpSN) (yellow sticks). The residues of 14-3-3c interacting with FC are represented as orange sticks and labeled in black.
(A) Orange spheres represent the Van der Waals surface of the residues engaging hydrophobic interactions with the hydrophobic diterpene moiety of FC.
(B) Black dashed lines indicate hydrogen bonds between FC and 14-3-3c residues S52 and D222. The hydrogen bond between FC and N677 of KAT1 peptide, labeled in red, is further indicated by a red arrow.
(C) Comparison of the structure adopted by FC in the ternary complex with 14-3-3c and the C terminus of KAT1 or H^+ pump. Upper panel: FC (cyan stick) establishes a hydrogen bond with the C-terminal Asn-677 of KAT1 (yellow stick) by means of the hydroxyl group at the C12 position of the diterpene ring, marked by an asterisk. Lower panel: FC (blue stick) interacts with the C-terminal valine residue of the H^+ pump (orange stick) by means of hydrophobic interactions. Spheres represent the van der Waals surface of the V side chain engaging hydrophobic interactions with the diterpene moiety of FC (redrawn from Würtele et al., 2003).
(D) Superimposition of the diterpene moiety of FC bound to KAT1 (cyan stick) and to H^+ pump (blue stick). Magenta arrow indicates the shift of the hydroxyl group at the C12 position caused by binding to KAT1. Asterisks indicate the hydroxyl group at the C12 position.

channel indeed responds to FC (Figures 5A and 5B, Table 1). Collectively, these data show that we have created an unorthodox internal 14-3-3 binding motif (i.e., not belonging to MODE I and II, but neither to MODE III since the phosphoserine is not at the penultimate position of the sequence anymore), which is the target of FC interaction and modulation of the channel current.

To further confirm that N677 is responsible for the required rearrangement of FC within the 14-3-3 cavity, we replaced this residue with valine (KAT1 N677V), i.e., the corresponding residue at the H^+ pump C terminus. First, we verified that the N677V mutation alone did not affect, as expected, the FC response of the current, when tested by electrophysiology (Figures 5A and 5B, Table 1). But, in the context of the elongated C terminus (KAT1 N677V/P678), the presence of the valine prevented the modulating effect of FC on the KAT1 current (Figures 5A and 5B, Table 1). These findings provide a strong functional validation for the role of asparagine in the newly identified spatial orientation adopted by FC within a 14-3-3 binding groove.

A Molecular Explanation for KAT1 Channel Rundown

When measured in excised inside-out patches, the KAT1 current undergoes a phenomenon referred to as rundown (Tang and Hoshi, 1999; Sottocornola et al., 2006). In this process, the voltage dependency of KAT1 is progressively shifted toward very negative voltages (>50 mV of left shift in the activation curve). Figure 6 shows that within 5 to 7 min from patch excision, the current becomes barely measurable and it is not possible to determine an accurate value of $V_{1/2}$. It was previously suggested that phosphorylation and 14-3-3 proteins could be involved in the rundown process (Tang and Hoshi, 1999). To test whether 14-3-3 proteins are directly responsible, we recorded the currents of the phosphomimic KAT1 S676D mutant in inside-out patches. We reasoned that this mutation, which stabilizes the KAT1:14-3-3 protein interaction, should prevent dissociation of 14-3-3 proteins from the channel after patch excision and hence counteract rundown. Figure 6 shows that this is the case: While the current of the wild-type channel progressively decreased over time, the current of the mutant remained about constant.

In this scenario, FC too should prevent KAT1 rundown by stabilizing its interaction with 14-3-3 proteins. To test this prediction, cells expressing wild-type KAT1 were treated with 10 μM FC 30 min prior to patch excision. Also in this case, the current did not undergo any rundown (Figure 6). Analysis of the $V_{1/2}$ values (Table 3) confirms that the fungal toxin acts by stabilizing the

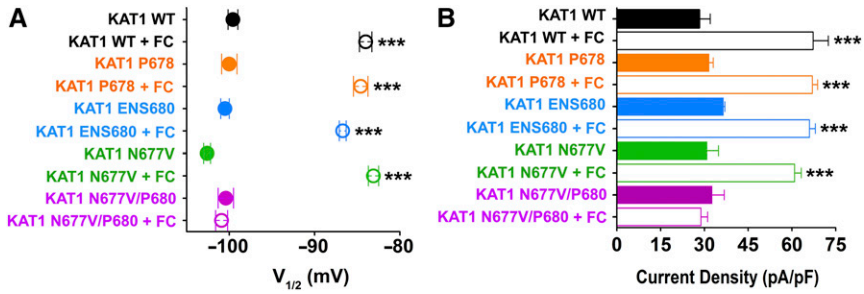

Figure 5. Functional Validation of the FC Orientation within the Ternary Complex.

Wild-type and mutant KAT1 channel currents were recorded by patch clamp in HEK 293T cells and further analyzed: Half activation potentials ($V_{1/2}$) **(A)** and tail current densities (pA/pF) **(B)**, in absence (solid symbols and bars) and presence (open symbols and bars) of 10 μM FC. KAT1 data are presented as means ± SE. Number of cells (*n*) was ≥ 8. Statistical analysis performed with *t* test (***P < 0.001).

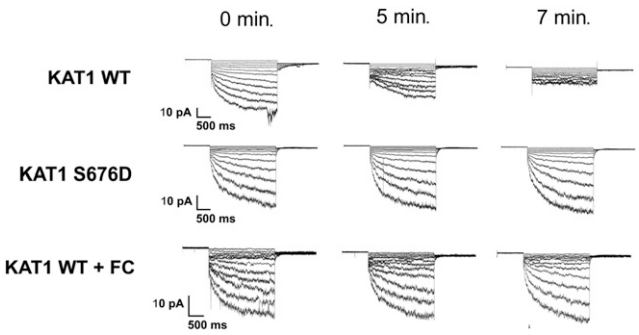

Figure 6. 14-3-3s and FC Prevent Rundown of KAT1 Current in Excised Patches.

Current traces recorded in HEK 293T cells expressing wild-type and S676D mutant KAT1 channels. The currents are shown at different times after patch excision (0, 5, and 7 min). Cells expressing wild-type KAT1 were pretreated with 10 μM FC for 30 min before patch excision. Shown traces are representative of $n = 3$ cells.

interaction between KAT1 wild-type channels and 14-3-3 proteins as much as the phosphomimic S676D mutant. Collectively, these results further support the view that 14-3-3 proteins directly regulate KAT1 channel activity by binding to the C terminus of KAT1. The results from the excised patches furthermore show that this occurs in the absence of other cytosolic elements.

DISCUSSION

Our study demonstrates that 14-3-3 proteins directly interact with KAT1 channels by binding with high affinity to a MODE III site at the very C-terminal end of the channel protein. The structural and biochemical data highlight the key role of phosphorylation of S676 at the penultimate position in the KAT1 sequence for 14-3-3 binding.

The structural data and physiological implications of these findings in KAT1 are best interpreted in the context of a concerted regulation of this channel with the H^+-ATPase by 14-3-3 proteins. On the part of the H^+-ATPase, it is long known that it has a MODE III type binding site for 14-3-3 proteins and that its occupation augments H^+ export (Ottmann et al., 2007; Duby and Boutry, 2009). This interaction is further stabilized by binding of the fungal toxin FC to this complex (Würtele et al., 2003). The present data now show that the scenario is, with some structural variations, paralleled in the KAT1 channel. Binding of 14-3-3 proteins to the MODE III binding site of KAT1 increases the conductance of the inward rectifier channel. As in the case of the H^+-ATPase, the KAT1:14-3-3 protein complex is also a target of FC. The fungal toxin binds to the latter and stabilizes it with the consequence that K^+ influx is further augmented.

The ability of FC to stabilize complexes in which 14-3-3 proteins bind partner proteins at a MODE III motive is well established (Würtele et al., 2003; Ottmann et al., 2009; Anders et al., 2013; Paiardini et al., 2014). Still, the fact that FC activates KAT1 by binding to its C terminus was quite surprising because KAT1 does not exhibit the typical MODE III binding motive for the toxin. The terminal asparagine in the channel should not allow toxin binding to this side. By contrast, the crystallographic data highlight that binding to such a noncanonical site is possible because of the structural adaptability of the FC molecule. While in the H^+-ATPase, FC stabilizes its complex with the 14-3-3 proteins via the interaction with a hydrophobic residue at the C-terminal end (Würtele et al., 2003), FC displays the same effect in the KAT1 channel by employing a so far unknown conformation. In this new pose, the interaction with the protein is stabilized by the polar residue at the C-terminal end of the channel. This apparent structural adaptability of FC is further underscored by experiments in which we extended the C terminus downstream of the FC binding site without losing FC binding. These results demonstrate that an effective binding site for the toxin is not restricted to a MODE III type motif at the C-terminal end of a protein. Hence, it is reasonable to assume that more undetected targets for this toxin will be identified in the future. Indeed, binding of FC to a non-MODE III motif has been reported also for the cystic fibrosis transmembrane conductance regulator (CFTR). However, in this case, FC binds in its standard conformation, which is made possible by the specific global architecture of the CFTR:14-3-3 complex (Stevers et al., 2016).

The noncanonical binding site of KAT1 for FC translates in a lower increment of the affinity in comparison to the H^+ pump (Würtele et al., 2003; Paiardini et al., 2014). In a physiological context, this difference in binding affinity might be relevant. It could account for the fact that channels have a much higher conductance than H^+-ATPases.

A number of mutations and control experiments underscore that binding of 14-3-3 proteins to KAT1 alters two properties of the channel, namely, its voltage dependency and maximal conductance. This implies a dual effect on channel function in which the shift in the voltage dependency can be assigned to an effect of the 14-3-3 protein on channel gating. The modulation of the maximal conductance could originate from an impact on the unitary

Table 3. Analysis of Currents Recorded in Inside-Out Configuration from Wild-Type and Mutant KAT1 Channels

	0 min			5 min			7 min		
	$V_{1/2}$	S	*n*	$V_{1/2}$	S	*n*	$V_{1/2}$	S	*n*
KAT1 WT	ND	ND	3	ND	ND	3	ND	ND	3
KAT1 S676D	−156.3 ± 1.5 mV	13.2 ± 1.4	3	−155.2 ± 1.7 mV	17.3 ± 1.4	3	−158.2 ± 1.7 mV	19.7 ± 1.5	3
KAT1 WT + FC	−157.5 ± 1.2 mV	16.2 ± 1.4	3	−159 ± 1.6 mV	22 ± 1.4	3	−156 ± 2 mV	22.3 ± 1.8	3

The 0, 5, and 7 min indicate time after patch excision. $V_{1/2}$, half activation potential; S, inverse slope coefficient; *n*, number of cells; WT, wild type.

channel conductance or alternatively from a modulation of channel trafficking. The results of the nonstationary noise analysis show that the unitary current of KAT1 is ~0.4 pA at –160 mV. This value is compatible with the small KAT1 conductance reported by single channel recordings in *Xenopus laevis* oocytes (Zei and Aldrich, 1998). Our finding that the channel current is not significantly affected by FC strongly suggests that FC interferes together with 14-3-3 proteins in the trafficking of the KAT1 protein to the plasma membrane. This is in good agreement with other reports, which have shown a control of cell surface expression of several other membrane proteins by 14-3-3 proteins (Mrowiec and Schwappach, 2006, Smith et al., 2011). They often do this by masking endoplasmic reticulum localization signals of proteins, which are then targeted to the plasma membrane (Smith et al., 2011). Since such endoplasmic reticulum retention sequences are not present in KAT1, it is possible that the channel harbors novel so far unknown sites. It is also possible that 14-3-3 proteins bind, as a dimer, simultaneously to KAT1 and other auxiliary proteins, which favor trafficking of the channel. The latter scenario has been reported for the surface expression of the Na^+/K^+-ATPase, where a 14-3-3-dependent recruitment of a kinase augments surface expression of the protein tandem (Efendiev et al., 2005). It also is not clear how 14-3-3 binding modulates KAT1 gating. However, it is well established that the C terminus is an active element for gating in KAT1 and channels with a similar architecture. This region contains the so-called KHA domain at the very C terminus, but also a C-linker and a CNBHD (Marten and Hoshi, 1997). These two domains constitute, even in channels that are not regulated by binding of cyclic nucleotides, a key region for gating control (Lolicato et al., 2011; Saponaro et al., 2014; Whicher and MacKinnon, 2016). Also, the aforementioned KHA domain is a potential target for a modulation of gating. Binding of 14-3-3 proteins to the KAT1 C terminus will move the individual domains on each subunit of the functional tetramer away from each other. This could trigger a conformational change in the C terminus, which may then be transmitted via long-range interactions to the channel pore domain. The structural details on these interactions are still unclear. In this context, the precise identification of the 14-3-3 binding site and its localization in KAT1 is now offering a valuable tool for unraveling the molecular details on how the 14-3-3 binding protein modulates protein surface expression and gating.

METHODS

Constructs

The cDNA encoding full-length KAT1 channel from *Arabidopsis thaliana* was cloned into the eukaryotic expression vector pcDNA 3.1 (Clontech Laboratories). Mutations were generated by site-directed mutagenesis (QuikChange site-directed mutagenesis kit; Agilent Technologies) and confirmed by sequencing.

Protein Expression and Purification

The cDNA fragment encoding residues 1 to 260 of tobacco (*Nicotiana tabacum*) 14-3-3c was cloned into pET-52b (EMD Millipore) downstream of a Strep (II) tag sequence. The plasmid was transformed into *Escherichia coli* BL21 Rosetta strain under ampicillin and chloramphenicol selection. Cells were grown at 37°C in Luria broth to 0.6 OD_{600} and induced with 0.4 mM isopropyl-1-thio-D-galactopyranoside. After 3 h, cells were collected by centrifugation (1367*g*, 30 min., 4°C), resuspended in ice-cold lysis buffer (150 mM NaCl, 100 mM Tris-Cl, pH 8, and 1 mM EDTA) with the addition of 1 mM β-mercaptoethanol, 10 μg/mL DNase, 0.25 mg/mL lysozyme, 100 μM phenylmethylsulfonyl fluoride, 5 μM leupeptin, and 1 μM pepstatin. The cells were sonicated on ice 20 times for 10 s each, and the lysate was cleared by centrifugation (25,673*g*, 30 min, 4°C). Protein was purified by affinity chromatography using StrepTrap HP columns (GE Healthcare) and eluted in 150 mM KCl, 30 mM HEPES, pH 7.4, and 2.5 mM desthiobiotin. The eluted protein was then loaded into HiLoad 16/60 Superdex 200 prep grade size exclusion column (GE Healthcare), which was equilibrated with 100 mM NaCl, 30 mM HEPES (pH 7.4), 10 mM $MgCl_2$, and 2 mM β-mercaptoethanol. All purification steps were performed at 4°C and monitored using the AKTApurifier UPC 10 fast protein liquid chromatography system (GE Healthcare). The protein purity was confirmed by SDS-PAGE.

Isothermal Titration Calorimetry

Measurements were performed at 25°C using a VP-ITC MicroCalorimeter (MicroCal; Malvern Instruments). The volume of sample cell was 1.4 mL; the reference cell contained water. CPnP or CPP (500 μM) was titrated using injection volumes of 10 μL into a solution containing 14-3-3c (50 μM) and, when present, FC (250 μM). Calorimetric data were analyzed with Origin software (version 7, MicroCal) and equations were described for the single-site binding model (Wiseman et al., 1989).

Crystallization, Data Collection, Phasing, and Refinement

14-3-3c (10 mg/mL, 0.3 mM) was cocrystallized with YFSpSN peptide (CPP: 3.5 mg/mL, 5 mM) or with HLYFSpSN peptide (CPP7: 4.8 mg/mL, 5 mM). Well diffracting crystals were obtained using the sitting-drop vapor diffusion method at 4°C with 30% PEG 400, 0.2 M ammonium acetate (pH 7.0), 0.1 M sodium citrate (pH 4.4), 10 mM DTT, and 5% glycerol for the 14-3-3c:YFSpSN complex, and 32% PEG 400, 0.2 M ammonium acetate (pH 7.0), 0.1 M sodium citrate (pH 4.4), 10 mM DTT, and 5% glycerol for the 14-3-3c:HLYFSpSN complex. Cocrystals of the 14-3-3c:YFSpSN:FC ternary complex grew in sitting-drop vapor diffusion experiments with 0.1 M potassium thiocyanate and 30% (w/v) PEG MME 2000, at 4°C. The concentration of the protein and the ligands were as follows: 14-3-3c (10 mg/mL, 0.3 mM), YFSpSN peptide (3.5 mg/mL, 5 mM), and FC (5 mM).

Crystals were mounted in fiber loops and directly flash cooled in liquid nitrogen. X-ray diffraction data from protein:peptide binary complexes and protein:peptide:FC ternary complex were collected at the European Synchrotron Radiation Facility (Grenoble, France) with beamlines ID30A-3 and BM14, respectively. Diffraction data were reduced using XDS (Karplus and Diederichs, 2012) and scaled with Aimless (Evans and Murshudov, 2013), as implemented in the CCP4 program package (Winn et al., 2011). The structures of the binary and ternary complexes were solved by molecular replacement with Phaser (McCoy et al., 2007) using the coordinates of the 14-3-3c:H^+ pump peptide complex (PDB: 1O9D) as a search model (Würtele et al., 2003). The electron density maps calculated using these preliminary phases were improved by manually correcting and/or rebuilding the initial models. Iterative cycles of restrained refinement with Phenix (Adams et al., 2010) and Refmac5 (Vagin et al., 2004) and model building with Coot (Emsley et al., 2010) were accomplished. The final models were validated with MolProbity (Chen et al., 2010).

Electrophysiology

The plasmid containing cDNA of wild-type and mutant KAT1 channels was cotransfected for transient expression into HEK293T cells with a plasmid containing cDNA of GFP. One day after transfection, GFP-expressing cells

were selected for patch-clamp experiments either in whole-cell configuration or inside-out. The experiments were conducted at room temperature. The pipette solution in whole-cell experiments contained 10 mM NaCl, 130 mM KCl, 1 mM EGTA, 2 mM ATP (magnesium salt), 5 mM HEPES (pH 7.2); the extracellular bath solution in whole-cell experiments contained 115 mM NaCl, 20 mM KCl, 1.8 mM $CaCl_2$, 0.5 mM $MgCl_2$, and 5 mM HEPES (pH 7.4). For inside-out experiments, the pipette solution contained 140 mM KCl, 2 mM $MgCl_2$, and 10 mM HEPES (pH 7.2). The intracellular bath solution contained 140 mM KCl, 2 mM $MgCl_2$, 10 mM HEPES, and 2 mM EGTA (pH 7.2). CPP was added (10 μM) to the pipette solution in whole-cell experiments. FC was added (10 μM) to the bath solution 30 min before starting both whole-cell and inside-out recordings. Whole-cell measurements of KAT1 channels were performed using a voltage clamp protocol consisting of a holding voltage of –30 mV and steps from –10 to –175 mV (15-mV interval). Tail currents were recorded at –70 mV. Whole-cell measurements of KAT2 channels were performed using a voltage clamp protocol consisting of a holding voltage of –30 mV and steps from –60 to –220 mV (20-mV interval). Inside-out measurements were performed using a voltage clamp protocol consisting of a holding voltage of –30 mV and steps from –40 to –205 mV (15-mV interval). Tail currents were recorded at –70 mV.

Data Analysis

Data were acquired at 1 kHz using an Axopatch 200B amplifier and pClamp10.5 software (Axon Instruments). Data were analyzed offline using Clampfit 10.5 (Molecular Devices) and Origin 16 (OriginLab). Activation curves were analyzed by the Boltzmann equation, y = 1/{1+exp[(V−V1/2)/s]}, where y is fractional activation, V is voltage, $V_{1/2}$ half-activation voltage, and s the inverse slope factor (mV) (Sottocornola et al., 2006). Mean activation curves were obtained by fitting individual curves from each cell to the Boltzmann equation and then averaging all curves obtained.

For noise analysis, KAT1 channels were measured in the whole-cell configuration as in Figure 3A. Channels were activated 100 times by 500-ms-long hyperpolarizing voltage step from –40 to –160 mV with 1.5-s-long intervals. Data were low pass filtered at 1 kHz. Raw data were imported into MATLAB to calculate the mean current I(t), the current differences between successive traces $y_n(t)$, the mean current differences Y(t), and the variance of the current differences $\sigma^2(t)$. $y_n(t)$, Y(t), and $\sigma^2(t)$ were calculated with the following equations (Liu et al., 2016):

$$y_n(t) = \frac{I_n(t) - I_{n+1}(t)}{2} \quad (1)$$

$$Y(t) = \frac{1}{M-1} \sum_{n=1}^{M} y_n(t) \quad (2)$$

$$\sigma^2(t) = \frac{2}{M-1} \sum_{n=1}^{M} (y_n(t) - Y(t))^2 \quad (3)$$

where *n* is the trace index and *M* the total number of traces collected. The variances were plotted against the mean current *I* and fitted with the following parabolic function (Liu et al., 2016):

$$\sigma^2(I) = i \cdot I - \frac{I^2}{N} + {\sigma_b}^2 \quad (4)$$

where *i* represents the single channel current, *N* the total number of channels, and ${\sigma_b}^2$ the background noise. Data were fitted with the constrain that ${\sigma_b}^2$ is ≥ 0.

Accession Numbers

Coordinates and structure factors have been deposited in the Protein Data Bank (PDB) under accession codes 5NWJ (14-3-3c:HLYFSpSN complex), 5NWI (14-3-3c:YFSpSN complex), and 5NWK (14-3-3c:YFSpSN:FC complex).

Supplemental Data

Supplemental Figure 1. Electron density maps for CPPs bound to 14-3-3c.

Supplemental Figure 2. Crystal structure of 14-3-3c in complex with two different CPPs and functional validation of the different position of F674.

Supplemental Figure 3. Electron density maps for 14-3-3c ligands in the 14-3-3c:CPP:FC ternary complex.

Supplemental Figure 4. Crystal packing of the 14-3-3c:CPP:FC complex.

Supplemental Figure 5. Thermodynamics parameters of CPP binding to 14-3-3c obtained by isothermal titration calorimetry.

Supplemental Figure 6. KAT2 channel does not respond to FC.

ACKNOWLEDGMENTS

We thank Marco Tomasi for technical help with the patch clamp recordings. This work was partly supported by MIUR PRIN (Programmi di Ricerca di Rilevante Interesse Nazionale) 2015 (2015795S5W), Schaefer Research Scholars Program from Columbia University, New York, to A.M., and European Research Council 2015 Advanced Grant (AdG) 695078 noMAGIC to A.M. and G.T.

AUTHOR CONTRIBUTIONS

A.S. designed and performed the research, analyzed the data, and contributed to the writing. A.P. and O.R. performed the research. A.C.-S. analyzed the data and contributed to the writing. M.N. designed the research, analyzed the data, and contributed to the writing. G.T. and A.M. designed the research, analyzed the data, and wrote the manuscript.

Received May 25, 2017; revised August 31, 2017; accepted September 27, 2017; published September 29, 2017.

REFERENCES

Adams, P.D., et al. (2010). PHENIX: a comprehensive Python-based system for macromolecular structure solution. Acta Crystallogr. D Biol. Crystallogr. **66:** 213–221.

Aducci, P., Marra, M., Fogliano, V., and Fullone, M.R. (1995). Fusicoccin receptors: perception and transduction of the fusicoccin signal. J. Exp. Bot. **46:** 1463–1478.

Anders, C., et al. (2013). A semisynthetic fusicoccane stabilizes a protein-protein interaction and enhances the expression of K^+ channels at the cell surface. Chem. Biol. **20:** 583–593.

Blatt, M.R. (2000). Cellular signaling and volume control in stomatal movements in plants. Annu. Rev. Cell Dev. Biol. **16:** 221–241.

Chen, V.B., Arendall III, W.B., Headd, J.J., Keedy, D.A., Immormino, R.M., Kapral, G.J., Murray, L.W., Richardson, J.S., and Richardson, D.C. (2010). MolProbity: all-atom structure validation for macromolecular crystallography. Acta Crystallogr. D Biol. Crystallogr. **66:** 12–21.

Duby, G., and Boutry, M. (2009). The plant plasma membrane proton pump ATPase: a highly regulated P-type ATPase with multiple physiological roles. Pflugers Arch. **457:** 645–655.

Efendiev, R., Chen, Z., Krmar, R.T., Uhles, S., Katz, A.I., Pedemonte, C.H., and Bertorello, A.M. (2005). The 14-3-3 protein translates the NA^+,K^+-ATPase alpha1-subunit phosphorylation signal into binding and activation of phosphoinositide 3-kinase during endocytosis. J. Biol. Chem. **280:** 16272–16277.

Ehrhardt, T., Zimmermann, S., and Müller-Röber, B. (1997). Association of plant K+(in) channels is mediated by conserved C-termini and does not affect subunit assembly. FEBS Lett. **409:** 166–170.

Emsley, P., Lohkamp, B., Scott, W.G., and Cowtan, K. (2010). Features and development of Coot. Acta Crystallogr. D Biol. Crystallogr. **66:** 486–501.

Evans, P.R., and Murshudov, G.N. (2013). How good are my data and what is the resolution? Acta Crystallogr. D Biol. Crystallogr. **69:** 1204–1214.

Johnson, C., Crowther, S., Stafford, M.J., Campbell, D.G., Toth, R., and MacKintosh, C. (2010). Bioinformatic and experimental survey of 14-3-3-binding sites. Biochem. J. **427:** 69–78.

Karplus, P.A., and Diederichs, K. (2012). Linking crystallographic model and data quality. Science **336:** 1030–1033.

Liu, C., Xie, C., Grant, K., Su, Z., Gao, W., Liu, Q., and Zhou, L. (2016). Patch-clamp fluorometry-based channel counting to determine HCN channel conductance. J. Gen. Physiol. **148:** 65–76.

Lolicato, M., et al. (2011). Tetramerization dynamics of C-terminal domain underlies isoform-specific cAMP gating in hyperpolarization-activated cyclic nucleotide-gated channels. J. Biol. Chem. **286:** 44811–44820.

Marrè, E. (1979). Fusicoccin: a tool in plant physiology. Annu. Rev. Plant Physiol. **30:** 273–288.

Marten, I., and Hoshi, T. (1997). Voltage-dependent gating characteristics of the K+ channel KAT1 depend on the N and C termini. Proc. Natl. Acad. Sci. USA **94:** 3448–3453.

McCoy, A.J., Grosse-Kunstleve, R.W., Adams, P.D., Winn, M.D., Storoni, L.C., and Read, R.J. (2007). Phaser crystallographic software. J. Appl. Cryst. **40:** 658–674.

Mrowiec, T., and Schwappach, B. (2006). 14-3-3 proteins in membrane protein transport. Biol. Chem. **387:** 1227–1236.

Ottmann, C., Marco, S., Jaspert, N., Marcon, C., Schauer, N., Weyand, M., Vandermeeren, C., Duby, G., Boutry, M., Wittinghofer, A., Rigaud, J.-L., and Oecking, C. (2007). Structure of a 14-3-3 coordinated hexamer of the plant plasma membrane H^+-ATPase by combining X-ray crystallography and electron cryomicroscopy. Mol. Cell **25:** 427–440.

Ottmann, C., Weyand, M., Sassa, T., Inoue, T., Kato, N., Wittinghofer, A., and Oecking, C. (2009). A structural rationale for selective stabilization of anti-tumor interactions of 14-3-3 proteins by cotylenin A. J. Mol. Biol. **386:** 913–919.

Paiardini, A., Aducci, P., Cervoni, L., Cutruzzolà, F., Di Lucente, C., Janson, G., Pascarella, S., Rinaldo, S., Visconti, S., and Camoni, L. (2014). The phytotoxin fusicoccin differently regulates 14-3-3 proteins association to mode III targets. IUBMB Life **66:** 52–62.

Saponaro, A., Pauleta, S.R., Cantini, F., Matzapetakis, M., Hammann, C., Donadoni, C., Hu, L., Thiel, G., Banci, L., Santoro, B., and Moroni, A. (2014). Structural basis for the mutual antagonism of cAMP and TRIP8b in regulating HCN channel function. Proc. Natl. Acad. Sci. USA **111:** 14577–14582.

Smith, A.J., Daut, J., and Schwappach, B. (2011). Membrane proteins as 14-3-3 clients in functional regulation and intracellular transport. Physiology (Bethesda) **26:** 181–191.

Sottocornola, B., Gazzarrini, S., Olivari, C., Romani, G., Valbuzzi, P., Thiel, G., and Moroni, A. (2008). 14-3-3 proteins regulate the potassium channel KAT1 by dual modes. Plant Biol. (Stuttg.) **10:** 231–236.

Sottocornola, B., Visconti, S., Orsi, S., Gazzarrini, S., Giacometti, S., Olivari, C., Camoni, L., Aducci, P., Marra, M., Abenavoli, A., Thiel, G., and Moroni, A. (2006). The potassium channel KAT1 is activated by plant and animal 14-3-3 proteins. J. Biol. Chem. **281:** 35735–35741.

Stevers, L.M., Lam, C.V., Leysen, S.F.R., Meijer, F.A., van Scheppingen, D.S., de Vries, R.M.J.M., Carlile, G.W., Milroy, L.G., Thomas, D.Y., Brunsveld, L., and Ottmann, C. (2016). Characterization and small-molecule stabilization of the multisite tandem binding between 14-3-3 and the R domain of CFTR. Proc. Natl. Acad. Sci. USA **113:** E1152–E1161.

Tang, X.D., and Hoshi, T. (1999). Rundown of the hyperpolarization-activated KAT1 channel involves slowing of the opening transitions regulated by phosphorylation. Biophys. J. **76:** 3089–3098.

Vagin, A.A., Steiner, R.A., Lebedev, A.A., Potterton, L., McNicholas, S., Long, F., and Murshudov, G.N. (2004). REFMAC5 dictionary: organization of prior chemical knowledge and guidelines for its use. Acta Crystallogr. D Biol. Crystallogr. **60:** 2184–2195.

Whicher, J.R., and MacKinnon, R. (2016). Structure of the voltage-gated K^+ channel Eag1 reveals an alternative voltage sensing mechanism. Science **353:** 664–669.

Winn, M.D., et al. (2011). Overview of the CCP4 suite and current developments. Acta Crystallogr. D Biol. Crystallogr. **67:** 235–242.

Wiseman, T., Williston, S., Brandts, J.F., and Lin, L.N. (1989). Rapid measurement of binding constants and heats of binding using a new titration calorimeter. Anal. Biochem. **179:** 131–137.

Würtele, M., Jelich-Ottmann, C., Wittinghofer, A., and Oecking, C. (2003). Structural view of a fungal toxin acting on a 14-3-3 regulatory complex. EMBO J. **22:** 987–994.

Zei, P.C., and Aldrich, R.W. (1998). Voltage-dependent gating of single wild-type and S4 mutant KAT1 inward rectifier potassium channels. J. Gen. Physiol. **112:** 679–713.